ACS NANO

www.acsnano.org

ARTICLE

Ultrastrong and Bioactive Nanostructured Bio-Based Composites

Nitesh Mittal,[†,‡] Ronnie Jansson,[§] Mona Widhe,[§] Tobias Benselfelt,[‡,∥] Karl M. O. Håkansson,[⊥] Fredrik Lundell,[†,‡] My Hedhammar,*[,§] and L. Daniel Söderberg*[,†,‡]

[†]Linné FLOW Centre, Department of Mechanics, [‡]Wallenberg Wood Science Center, [§]Division of Protein Technology, School of Biotechnology, and [∥]Department of Fibre and Polymer Technology, KTH Royal Institute of Technology, SE-100 44 Stockholm, Sweden

[⊥]Innventia AB, P.O. Box 5604, SE-114 86 Stockholm, Sweden

Supporting Information

ABSTRACT: **Nature's design of functional materials relies on smart combinations of simple components to achieve desired properties. Silk and cellulose are two clever examples from nature—spider silk being tough due to high extensibility, whereas cellulose possesses unparalleled strength and stiffness among natural materials. Unfortunately, silk proteins cannot be obtained in large quantities from spiders, and recombinant production processes are so far rather expensive. We have therefore combined small amounts of functionalized recombinant spider silk proteins with the most abundant structural component on Earth (cellulose nanofibrils (CNFs)) to fabricate isotropic as well as anisotropic hierarchical structures. Our approach for the fabrication of bio-based anisotropic fibers results in previously unreached but highly desirable mechanical performance with a stiffness of ∼55 GPa, strength at break of ∼1015 MPa, and toughness of ∼55 MJ m^{-3}. We also show that addition of small amounts of silk fusion proteins to CNF results in materials with advanced biofunctionalities, which cannot be anticipated for the wood-based CNF alone. These findings suggest that bio-based materials provide abundant opportunities to design composites with high strength and functionalities and bring down our dependence on fossil-based resources.**

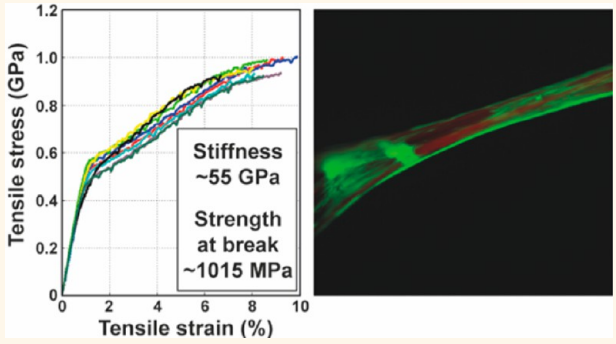

KEYWORDS: *bio-based materials, strength, toughness, specific affinity, cell adhesion*

Lightweight structural materials from renewable resources offer properties that can surpass the performance of their components by several orders of magnitude.[1] Silk and cellulose are two excellent examples of high-performance bio-based materials[2−6] that can provide a basis for technological developments supporting a sustainable society by replacing the fossil-based composites. Due to its attractive mechanical properties (high tensile strength and extensibility)[7,8] and biocompatibility,[9−11] spider silk proteins have demonstrated the potential for numerous applications.[12−15] The recently discovered option to obtain bioactive recombinant silk through combination of the spider silk protein module with peptides or protein domains already at gene level further expedites the possibilities in the areas of biomedicine. Examples of functionalities that can be procured by the use of recombinant silk fusion proteins are cell-binding ability, specific affinity, and enzymatic activity.[16−21]

To facilitate wider use of such bioactivities, there is a strong incentive to reduce the high cost of materials based on 100% silk proteins. One route to achieve this is to combine the silk proteins with a compatible building block that comes at a lower cost, can be produced in larger volumes, and preferably adds complementary functionality. Cellulose nanofibrils obtained from trees have received remarkable scientific and commercial attention lately as it is a renewable resource available in larger volumes, yielding materials combining several favorable features such as biodegradability and low toxicity along with impressive mechanical properties.[22] The high aspect ratio (>150) and stiffness (∼138 GPa) of the crystalline regions of cellulose nanofibrils (CNFs) make this material ideal as a reinforcing element in composites.[23−26] However, lack of bioactive nature is limiting its use in biomedical applications.[27] Integrating CNF with recombinant spider silk proteins (RSPs) will lead to future advanced products having properties that can benefit a wide range of applications, given the possibility to functionalize the material.[28]

Received: April 2, 2017
Accepted: May 5, 2017
Published: May 5, 2017

DOI: 10.1021/acsnano.7b02305
ACS Nano 2017, 11, 5148−5159

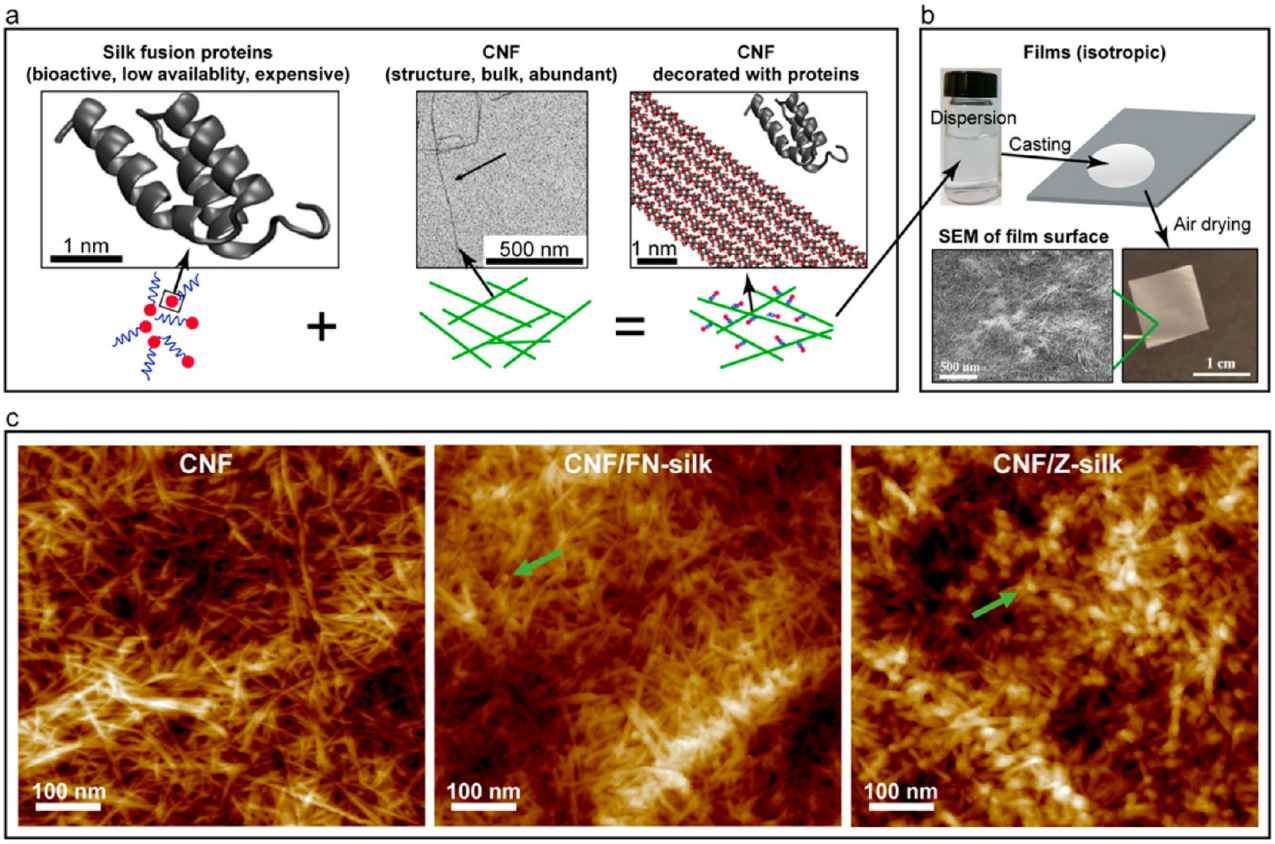

Figure 1. Formulation of composite isotropic films of CNF (90%) and silk (10%). (a) Schematics showing how the functionalized RSPs interact with and decorate the surface of CNF. Insets show scaled images. The atomic model shows a single fibril represented by aligned β-(1,4)-glucan chains (red and gray color, Nishiyama *et al.*[34]) together with a protein Z domain (gray color, Tashiro *et al.*[35]). Red color represents the functionalized domains attached to the silk (blue color). (b) Fabrication of anisotropic CNF films. Optical microscopy image of a CNF film prepared by the method of solvent casting. SEM image of the surface of a CNF film showing a dense network of fibrils with an apparently isotropic orientation. (c) AFM images of the film surfaces. Homogeneous distribution of proteins throughout the film surface in the form of small clusters of 3−10 nm can be seen (examples indicated by green arrows).

Inspired by the properties and functions obtained with recombinant spider silk fusion proteins, we have herein combined CNF with two types of silk fusion proteins: Z-silk and FN-silk. In Z-silk, the silk protein is fused to an affinity domain Z,[29] which adds the ability to selectively bind immunoglobulin G (IgG).[17] In FN-silk, the material is instead functionalized with an RGD-containing cell-binding motif from the extracellular matrix (ECM) protein fibronectin.[30] The thereby fabricated materials show surface bioactivity in the same way as materials based on pure silk fusion proteins, even when the composition is predominantly CNF (~90%). Furthermore, compared to other reported bio-based composites,[1,31] the nanstructured materials exhibit simultaneous outstanding stiffness (elastic modulus ~55 GPa), toughness ~55 MJ m^{-3} (strain-to-failure ~10%), and strength (strength at break ~1015 MPa).

RESULTS AND DISCUSSION

Fabrication of Isotropic Heirarchical Structures. We herein applied the concept of mixing CNF and RSP in a hydrocolloidal dispersion, where the stability of the dispersion is controlled by supramolecular interactions[26] (Figure 1a). For comparison of the molecular sizes of the different components, a schematic atomic model of the Z domain and the CNF β-(1,4)-glucan polymer chain is shown. A straightforward preparation process based on solvent casting has been applied to dispersions consisting of CNF (90%)/silk (10%) blends, where a free-standing film of a planar fibril network is obtained after evaporation of water (Figure 1b). Except for the simplicity, a key advantage of this technique is the capability to prepare large-area films with well-defined dimensions, which is not possible using other film-forming methods like dip- or spin-coating.[32] Structures of the films surfaces were analyzed using scanning electron microscopy (SEM) and atomic force microscopy (AFM), showing a dense web-like fibril network, where the CNF from the wood pulp fibers is clearly visible (Figure 1b,c). Individual CNFs are wriggled and physically entangled to each other, indicating strong fibril−fibril interactions (*e.g.*, hydrogen bonds, van der Waals interactions[33]) and/or a result of fibril flocculation due to the crowding factor/number density. When comparing the surface morphologies of the films prepared from CNF and CNF/silk dispersions, no clear difference is observed from SEM (Figure S1a,b). However, AFM reveals the presence of proteins in the form of small clusters homogeneously distributed throughout the dense CNF network (Figure 1c).

Functional Studies of Composite Films. Materials with specific affinity, that is, the ability to selectively sort out one type of molecule from a complex mixture, is essential in various applications, for example, purification of biomolecules such as antibodies. Immobilization of bioactive proteins, such as affinity modules, often relies on surface activation and blocking steps

DOI: 10.1021/acsnano.7b02305
ACS Nano 2017, 11, 5148−5159

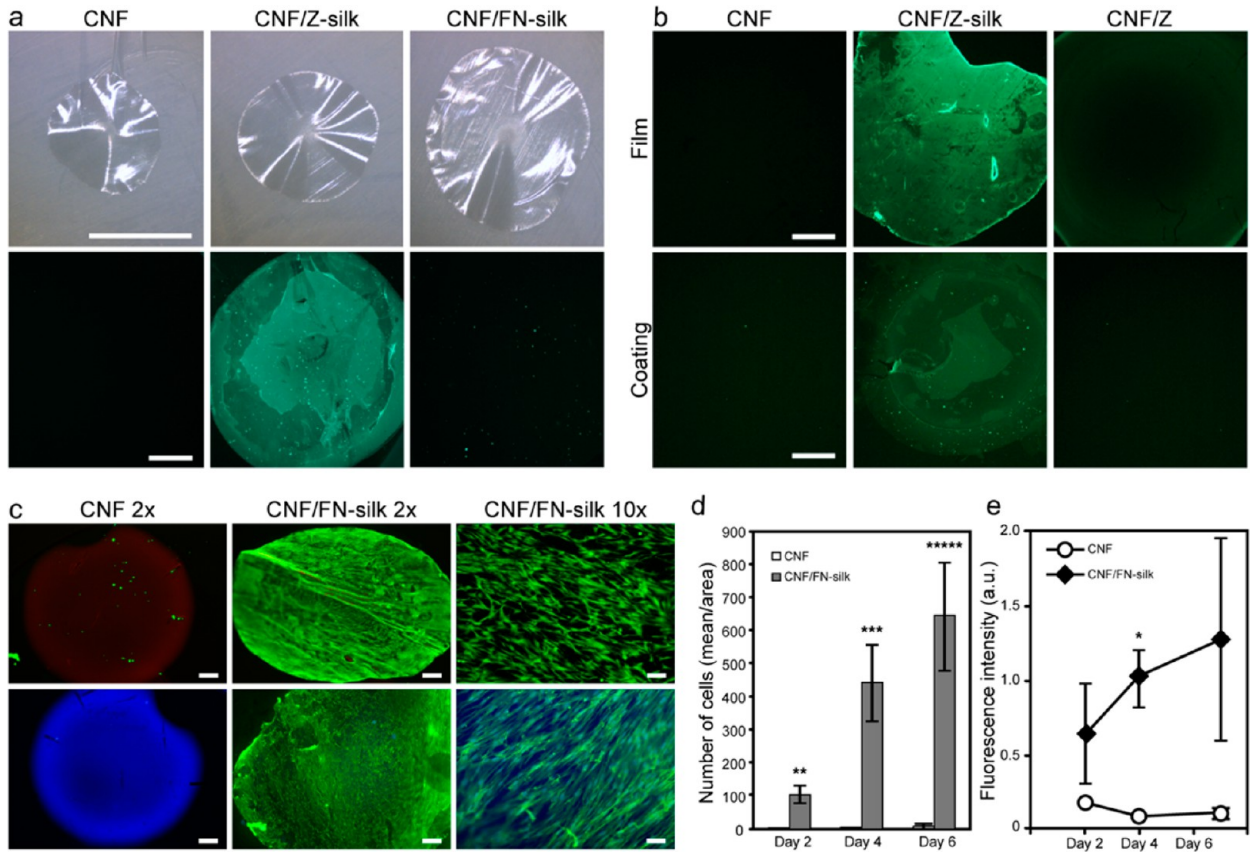

Figure 2. Functional studies of composite films show presence of bioactivity. (a) Optical microscopy images of CNF and composite CNF/silk films (top panel). Scale bar is 4 mm. Images from fluorescence microscopy visualizing the binding of fluorophore-labeled IgG (green, bottom panel). Scale bar is 1 mm. (b) Signal from IgG-fluorophore bound to a film casted from a mixture of CNF and the Z domain alone (CNF/Z), CNF premixed with Z-silk (CNF/Z-silk) or pure CNF, respectively, visualized by fluorescence microscopy (top panel). Visualization of IgG-fluorophore bound to a CNF film coated with the Z domain alone (CNF/Z), Z-silk (CNF/Z-silk), or noncoated (CNF) (bottom panel). Scale bars are 1 mm. (c) Human dermal fibroblasts cultured on films of CNF or CNF/FN-silk for 7 days. Top panel: live/dead staining (green, living cells; bright red, dead cells; dim red, autofluorescence from CNF). Bottom panel: F-actin staining (green, F-actin; blue, nuclei/autofluorescence from CNF). Scale bars 500 μm for 2× and 100 μm for 10×. (d) Number of HDMECs (mean + SD) per mm^2 on free-standing films of CNF (open bar) and CNF/FN-silk (gray bar), at different time points during culture, as evaluated by DAPI staining and manual counting of nuclei. Statistically significant differences according to Student's t test: $^{**}p < 0.01$, $^{***}p < 0.001$, and $^{*****}p < 0.00001$. (e) Representative Alamar blue viability graph of three independent experiments with HDMEC growing on CNF and CNF/FN-silk films (n = 3) during 1 week. Statistically significant differences according to Student's t test: $^{*}p < 0.05$. Error bars show standard deviation.

by the use of various chemicals in a sequential manner. For example, CNF was in a previous study conjugated with a short peptide using a set of reaction steps in order to display specific affinity toward human immunoglobulin G (hIgG).[36] Herein, we instead of chemical reactions utilize the silk module as a mild glue between an affinity domain and CNF. This approach offers a rapid and easy procedure for creation of bioactive materials. The chemical-free nature of this immobilization process preserves the fold and biofunctionality of the immobilized affinity domain. Theoretically, the design of the functionalized RSP allows for a high fraction of correctly oriented affinity molecules in the final material.

The herein fabricated CNF films were evaluated with respect to IgG-binding ability achieved by the combination with Z-silk. Although the macroscopic appearance of films made of CNF/silk are nearly identical to that of CNF (Figure 2a, top panel), a note should be made that there seems to be a tendency for both types of CNF/silk films to have a larger surface spreading on the Teflon sheets where they are casted than the corresponding CNF films. This is likely coupled to changes in wetting properties of the CNF dispersions due to the introduction of silk proteins. The IgG-binding ability of the films was evaluated using fluorophore-labeled IgG (Figure S2), which gives a clear green signal upon binding to the CNF/Z-silk film (Figure 2a, bottom-middle panel). The signal is distributed over the entire surface area of the CNF/Z-silk film, indicating a homogeneous structure of the composite. As a comparison, no signal from IgG binding can be seen for either the CNF or the CNF/FN-silk films (Figure 2a, bottom-left and right panel, respectively). Taken together, the signal from the CNF/Z-silk films implies that inclusion of Z-silk into the composite films adds a prominent IgG-binding ability. This, in turn, also implies that the Z domains of Z-silk are exposed outward in the CNF/Z-silk film and retain the native three-dimensional helical fold required for IgG binding.

In order to investigate if fusion to the silk module (4RepCT) in Z-silk is necessary to achieve IgG-binding ability of CNF composite materials, a control experiment was performed, where the silk module was excluded and CNF was instead casted into films after mixing with the Z domain alone. When analyzing such CNF/Z films, only a weak fluorescence signal can be detected, confirming very low binding of the labeled IgG

DOI: 10.1021/acsnano.7b02305
ACS Nano 2017, 11, 5148−5159

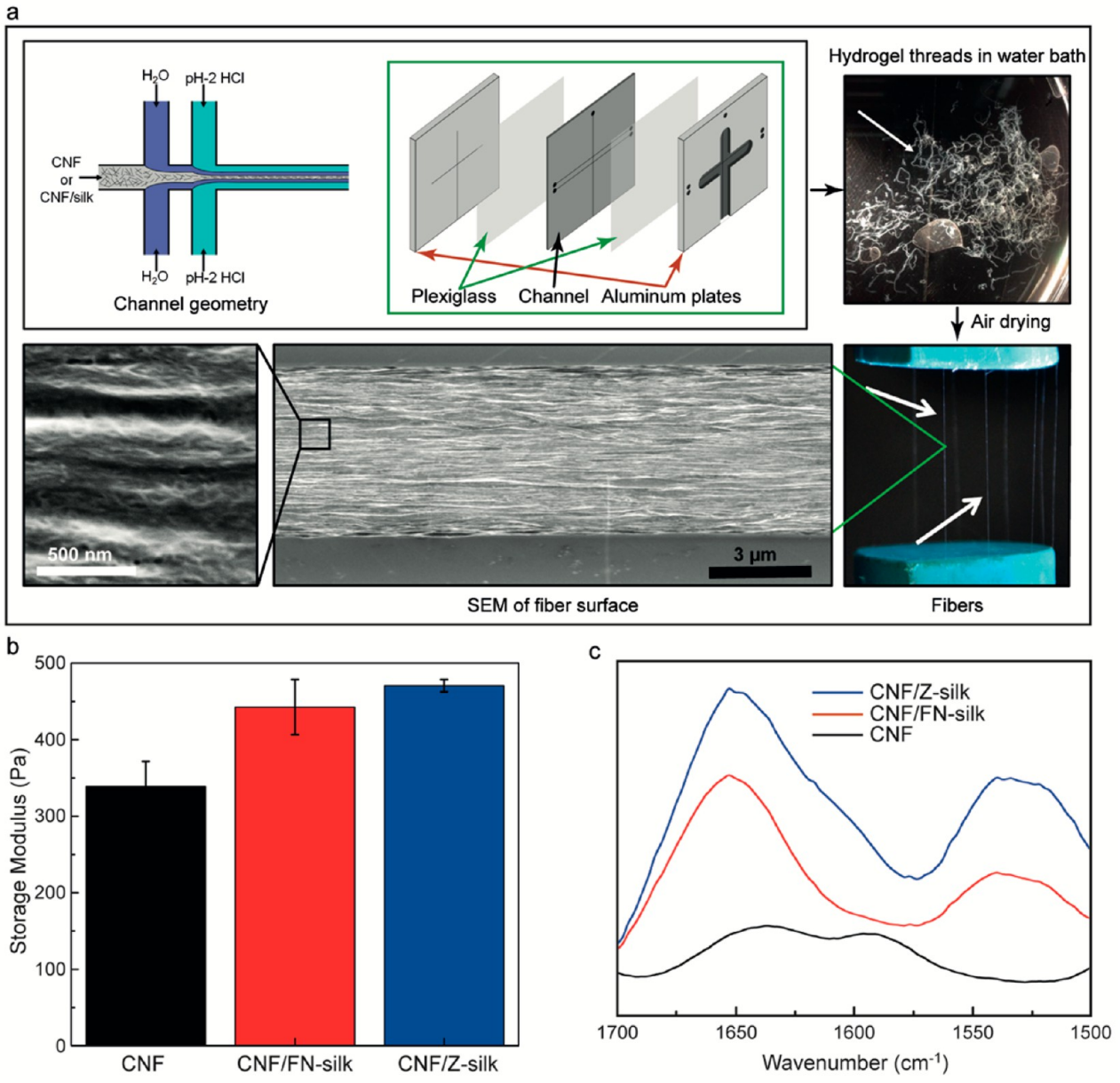

Figure 3. Formulation of composite anisotropic fibers of CNF (90%) and silk (10%). (a) Schematics showing the double flow-focusing geometry used for generation of fibers in the current study. The dispersion is extruded from the double flow-focusing geometry as hydrogel-like threads which are collected in a water bath. Optical microscopy image of fibers after air-drying while mounted between a quick clamp and illuminated by a polarized light source. The white arrows indicate the position of two fibers. SEM image of the surface of a CNF fiber with aligned structure of CNF fibrils generated with the double flow-focusing geometry. Inset shows a zoomed-in view of the fiber surface, where individual CNF fibrils are visible. (b) Average storage modulus (G') of CNF and CNF/silk dispersions obtained from rheological measurements. (c) Fourier transform infrared spectrum of the fibers fabricated from CNF and CNF/silk dispersions. The peaks between 1655−1640 cm^{-1} and 1540−1525 cm^{-1} in CNF/silk composite fibers correspond to the amide bands of proteins, which are related to their secondary structures.[42]

(Figure 2b, top-right panel). Thus, the difference in IgG affinity of the materials is obvious when comparing to the strong signal from CNF/Z-silk films (Figure 2b, top-middle panel). These results emphasize that covalent attachment of the Z domain to the silk module is absolutely necessary for the generation of composite CNF/Z-silk films with IgG-binding ability. This is probably due to the self-assembly of the silk module acting as an efficient and mild glue to the CNF, thereby connecting the covalently linked Z domain. On the contrary, when using the Z domain alone without the silk module, it will not stick to CNF and thus get washed away in subsequent handling steps. In addition, it can be speculated that a certain fraction of remaining Z domains will be denatured upon direct contact with CNF without the silk module at a distance and will thus not keep its folded state needed for IgG binding. To further investigate the role of the silk module for IgG binding in CNF/Z-silk materials, premade CNF films were coated with a solution of the Z domain alone and the Z-silk fusion protein. Again, CNF coated with the Z domain alone was then found to bind as little IgG as the control film made of pure CNF (Figure

DOI: 10.1021/acsnano.7b02305
ACS Nano 2017, 11, 5148−5159

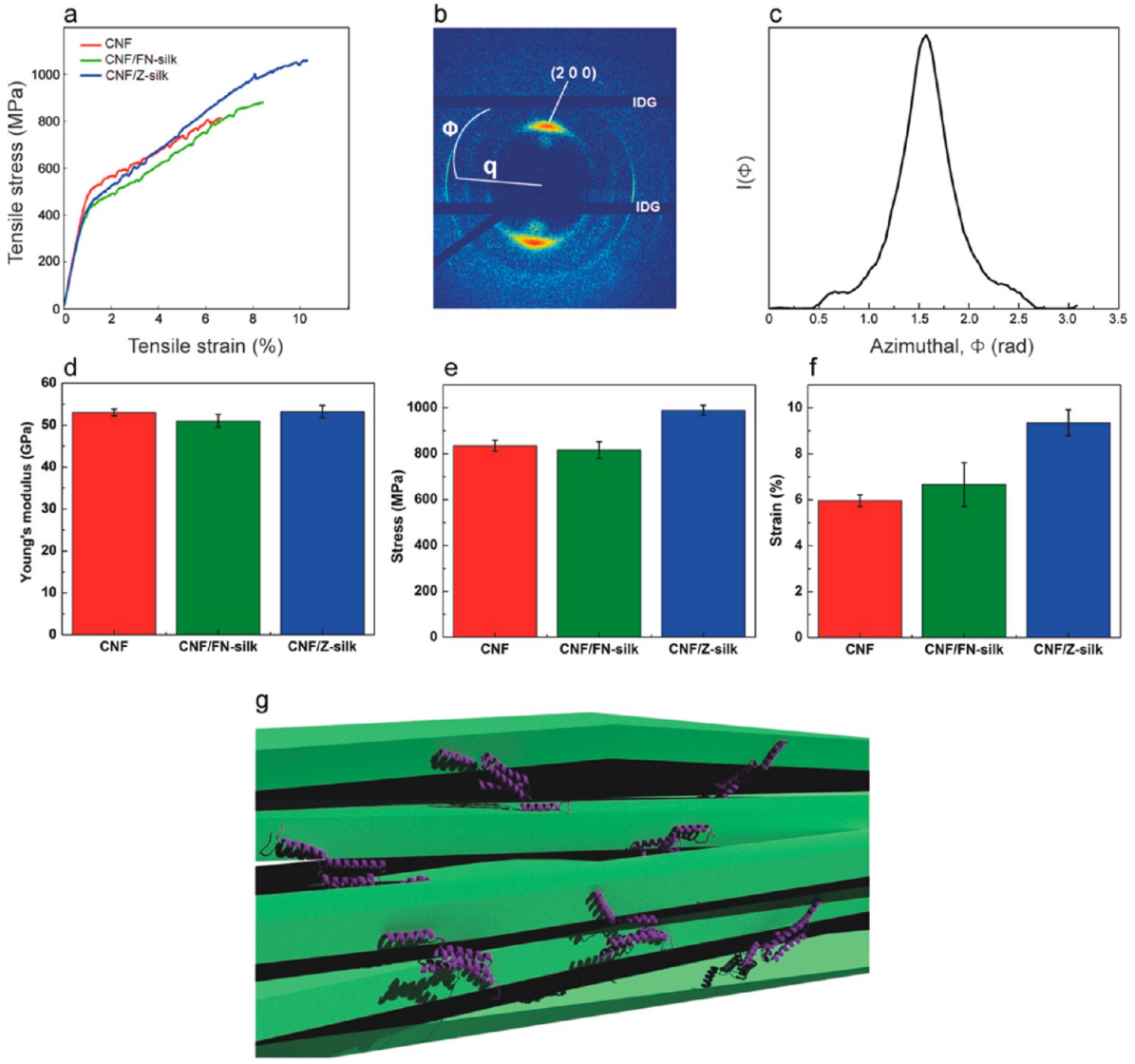

Figure 4. Mechanical and structural characterization of the fibers. (a) Tensile mechanical properties of CNF and CNF-silk fibers measured at 50% RH. (b) Wide-angle X-ray diffraction diffractogram of a CNF fiber, where IDG denotes the intermodular detector gap. (c) Azimuthal integration of the (200) scattering plane of the diffractogram shown in (b). (d) Young's modulus of CNF and CNF/silk fibers. (e) Stress at break of CNF and CNF/silk fibers. (f) Strain-to-failure of CNF and CNF/silk fibers. (g) Schematic representation of a CNF/silk fiber. Green, cellulose nanofibrils; purple, silk proteins.

2b, bottom-right and left panel, respectively), whereas CNF films coated with Z silk show a clear signal from bound IgG, although not as high as that for the composite film (Figure 2b, bottom-middle panel). This confirms that a covalent link between Z domain and the silk module is needed to firmly attach folded Z domains to CNF materials.

Nanocellulose, from different sources, has been used for formulation of scaffolds intended for usage in cell culture.[27] Specifically, hydrogels of CNF have been used for the encapsulation of cells (either from cell lines or tumor-derived cells) in a 3D environment.[37−39] Typically, a maintained viability of the encapsulated cells is then observed, confirming a good biocompatibility of CNF. However, direct interaction of cells with cellulose, that is, adhesion in a cell-matrix-like fashion, has not been shown, likely due to the lack of bioactive motifs in pure cellulose. By glutaraldehyde cross-linking of CNF extracted from plants, Mertaniemi *et al.*[40] could show an improved cell spreading on the threads after 1 week of culture.

Within this study, we evaluated how the inclusion of a silk protein fused to a cell-binding motif from fibronectin (FN-silk) could improve the ability of CNF-based materials to support culture of primary cells. First, we seeded human dermal fibroblasts (HDFs) onto the different films and traced the adhesion of cells by viability staining after 1 week (Figure 2c, top pannel). A complete coverage of living fibroblasts could be seen on the CNF/FN-silk films, whereas only very few cells were found on the films made of pure CNF, although these present cells were also viable. Attachment and morphology of the cells were therefore further investigated by staining for the cytoskeletal component F-actin. Fibroblasts cultured on CNF/FN-silk films exhibited well-developed stress fibers and elongated morphology, whereas almost no cells were found attached to the CNF film made without FN-silk (Figure 2c, bottom panel). Thus, fibroblasts seem to be unable to attach to the pure CNF film, but in a composite material with FN-silk, the cells exhibit excellent attachment, survival, and spreading.

DOI: 10.1021/acsnano.7b02305
ACS Nano 2017, 11, 5148−5159

This indicates that the cell-binding motif FN fused to silk is well-presented in the composite films, in a way that can be recognized by cell surface receptors mediating adhesion (*e.g.*, integrins). To further challenge the system, the films were seeded with microvascular endothelial cells (HDMEC), a cell type known to be dependent on ECM proteins for adhesion. The number of cells adhered to the different films were counted 2, 3, and 6 days after seeding (Figure 2d), confirming that inclusion of the FN-silk protein is necessary in order to obtain a material that promotes cell adhesion. Endothelial cells were well spread out after 1 week culture on the CNF/FN-silk films, displaying distinct stress fibers, both indications of well-established cell attachement (Figure S3). In contrast, on CNF films, no cells showed these characteristics. It is worthwhile to note that surface roughness, which also influences response of cells toward any surface, does not vary much for the films fabricated with and without proteins. The mean roughness values for the films of CNF and CNF/FN-silk films were 4.3 and 7.58 nm, respectively. In order to verify that those cells that are adhered to the films remain proliferative, an Alamar blue viability assay was also performed during 1 week of culture (Figure 2e).

Fabrication of Anisotropic Heirarchical Structures. Within the herein fabricated films, the fibril orientation is isotropic in the plane. In order to obtain anisotropic structure, that is, fibrils oriented along the longitudinal direction, we utilized a recently invented fabrication method for making fibers of CNF[41] and adapted the process for making CNF/silk composites (Figure 3a). Highly oriented fibers are then obtained using a flow-assisted alignment and assembly approach based on surface-charge-controlled gel transition. For the present experiments, we used a double flow-focusing setup, with a core flow of CNF or CNF/silk dispersions and two surrounding sheath flows, where the first sheath consists of deionized water (pH ∼ 5.6) and the second sheath consists of hydrochloric acid (HCl) (0.01 M, pH ∼ 2). The role of the first sheath is to prevent buildup at the channel walls, whereas the second sheath aligns the CNF (or CNF with silk proteins) in the dispersion with the help of elongational (contracting) flow-field and locks them together into a gel-like (arrested state) format. To achieve highly aligned fibrils, the timing of this process is of great importance. The fibrils in the dispersion are fairly free to rotate and thus will try to de-align due to electrostatic repulsive forces and Brownian diffusion. Therefore, before the alignment is lost, there is a need to reduce the electrostatic forces between the fibrils and lock the aligned structure. This is achieved through hydrogen ions provided from the HCl, which diffuse into the dispersions and initiate a gel transition by neutralizing the charged carboxyl groups on the fibrils' surface. This approach allows fabrication of fibers with a highly ordered (aligned) arrangement of fibrils (Figure 3a). Parallel and bundled arrangement of the fibrils can be seen by scanning electron microscopy (SEM) analysis of the CNF fiber surface. Individual fibrils in a very compact network are visible from the zoomed-in view of the fiber surface.

In order to fabricate composite fibers, a dispersion of CNF (90%) and silk proteins (10%) was prepared directly before being subjected to flow-focusing. The integrality of the silk proteins with CNF in the dispersions was assessed with the rheological measurements, which showed that the presence of silk proteins increased the stiffness of CNF dispersions significantly (Figure 3b and Figure S4). The inclusion of FN and Z-silk proteins gave ∼30−35% higher averaged G' values than the corresponding CNF dispersions. From these dispersions, CNF/Z- and CNF/FN-silk fibers with a surface morphology similar to that of pure CNF was obtained (Figure S5). Fourier transform infrared (FTIR) spectroscopy was used in order to verify that the silk proteins were integrated into the fibers and not washed away in the following water bath. Prominent peaks at regions corresponding to amide I (∼1650 cm^{-1}) and amide II (∼1530 cm^{-1}) confirm the presence of silk proteins[42] in the CNF/silk fibers (Figure 3c) but are lacking in the pure CNF fibers. However, due to the broadness of the peaks, it is not possible to determine the proportions of the silk proteins that have transformed into β-sheet conformation.[17,42,43]

Elevated Tensile Strength of the Fibers. The mechanical properties of the as-prepared oriented fibers were characterized in terms of stiffness, strength at break, and strain-to-failure using tensile testing. CNF fibers revealed an average modulus of 52.8 ± 0.7 GPa, strength at break of 830 ± 24 MPa, and a strain-to-failure of around 6% (toughness ∼ 37 MJ/m^3) (Figure 4a−f). The highest strength at break of a CNF fiber reached 854.6 MPa. In the past, many attempts have been made to produce fibers from the assembly of CNF by the methods of mechanical drawing or spinning.[41,44−47] However, the fibers with best mechanical properties reported were limited to a modulus of 15−35 GPa, strength at break of 200−500 MPa, and strain-to-failure of 1−5%. Hence, it is worthwhile to mention that this is the highest strength ever achieved for fibers fabricated from CNF, and to our knowledge, the current results also set a record for overall mechanical performances of fibers from bio-based materials.[1]

The fibril orientation in the CNF fiber was further characterized using wide-angle X-ray diffraction (WAXS) (Figure 4b). The (200) reflection of cellulose I, which generally is used to study the orientation of cellulose crystals, is here used to track the orientation of CNF, as crystals are aligned in the fibril direction.[41] The fibril orientation in the CNF fiber was calculated using the following equation based on azimuthal breadth analysis:[48]

$$f_c = (180° - \text{fwhm})/180° \quad (1)$$

where f_c represents the orientation index. Full width at half-maximum (fwhm) is determined from the azimuthal profile of the (200) plane (Figure 4c), and the calculated f_c value for our fiber is 0.86. The value of f_c in this study (0.86) is slightly higher than earlier reported values for cellulose fibers formed by the assembly of wood-based CNF (f_c varies from 0.55 to 0.83).[44−47] Lundahl *et al.*[45] reported a modulus of 21 GPa with f_c of 0.83, whereas Torres-Rendon *et al.* reported a modulus of 33 GPa with a similar value of f_c. The scatter in data between modulus and f_c values suggests that, apart from the degree of alignment, other structural characteristics of the macroscopic fibers as well as chemical interactions between the constituent fibrils play an important role in determining the mechanical properties of the fibers. The higher values of strength obtained for the fibers in this study could also be related to the smaller dimensions of the current fibers, which decreases the probability of defects leading to a earlier breakage.[49]

Encouraged by the outstanding performance of the CNF fibers, we also evaluated if the mechanical properties of composite fibers were affected by being prepared in the presence of silk fusion proteins. Fibers of CNF/FN-silk showed comparable properties, with a modulus of 50.2 ± 1.3 GPa,

DOI: 10.1021/acsnano.7b02305
ACS Nano 2017, 11, 5148−5159

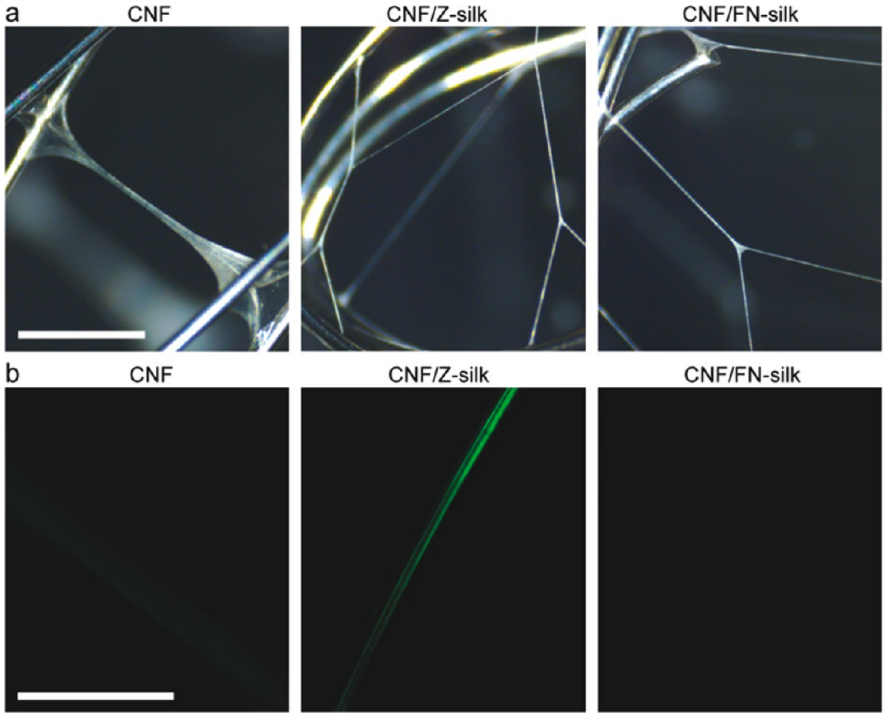

Figure 5. Affinity properties of the fibers. (a) Macroscopic appearance of CNF and composite CNF/silk fibers as viewed by optical microscopy. Scale bar is 4 mm. (b) Ability of CNF/Z-silk fibers to bind IgG-fluorophore (green) visualized using fluorescence microscopy. Scale bar is 0.5 mm.

strength at break of 812.5 ± 25.4 MPa, and strain-to-failure of 6−8% (toughness ∼43 MJ m^{-3}) (Figure 4d−f). Somewhat surprisingly, fibers of CNF/Z-silk show higher (reaching 10%) strain-to-failure (toughness ∼55 MJ m^{-3}) and strength (on the order of ∼1 GPa: 978.8 ± 37.5 MPa) than the pure CNF fibers, whereas the modulus (53.6 ± 1.8 GPa) is similar. One possible explanation is that the addition of Z-silk proteins, which harbor a stably folded helical Z domain fused to the silk, promotes bonding between CNF fibrils and enhances the overall strength, as hypothesized in a recent study by Malho and co-workers.[26] However, this effect is less evident for the CNF/FN-silk fibers, in which the silk modules are instead fused to only a short peptide. In the seminal work of Xia *et al.*[7] and Lazaris *et al.*,[8] a modulus of 21 and 12 GPa and ultimate strength of 508 and 259 MPa have been reported for artificially spun fibers of silk proteins alone. It is noteworthy that the modulus (∼55 GPa) and strength (∼1000 MPa) of the CNF/silk fibers designed in this study are 2−4.5 times higher, whereas at the same time, the toughness (∼55 MJ m^{-3}) is maintained.[7,8] More importantly, the results from these tensile tests of fibers are in good agreement with the rheology measurements on corresponding gels (arrested state) of CNF and CNF/silk dispersions (Figure 3b), where an increased G' indicates the enhanced interactions between the fibrils in the presence of silk proteins. The tensile test results along with FTIR measurements (Figure 3c) also indicate that the silk proteins are not merely present along with the CNF in the dispersions, but rather they interact and stick well to the surface of CNF.

Another interesting observation is that silk proteins can form stable dispersions with charged CNF that can be processed, that is, subjected to flow-fields, despite the fact that shear forces are known to promote self-assembly of the silk proteins.[50,51] The capability of CNF as a stabilizing agent has recently been demonstrated for carbon nanotubes[52] and thus shows a viable route of using it as a general tool for the fabrication of high-performance nanostructured materials. This capability is also supported by the results obtained with our flow-focusing setup, where the CNF/silk dispersions can easily be processed to fabricate fibers with well-ordered nanoarchitecture. The flow-focusing approach provides a well-defined elongational flow-field which, together with the controlled decrease in pH, could lead to *in situ* transition of the silk proteins from α-helix to β-sheet[50] and thereby promote stable interactions (*e.g.*, hydrogen bonds) with the CNF. Apart from the cellulose−cellulose interactions between the fibrils that contribute to the stiffness of a pure CNF fiber, the silk proteins distributed on the CNF give rise to silk interactions bridging the CNF (Figure 4g), which results in significantly increased maximum strain. The obtained hybrid material thus maintains a stiffness given by the cellulose interactions, and when CNF−CNF joints fail during uniaxial loading, the coating of silk proteins provides resilient bonds between neighboring fibrils, allowing load transfer at higher strain. This effect is particularly evident from the mechanical performance of the CNF/Z-silk fibers, possibly due to protein interaction provided by the more bulky Z domains.

Functional Studies of Composite Fibers. Similar to films, the fabricated fibers were also tested with respect to functionality. After air-drying, both CNF/Z-silk and CNF/FN-silk fibers have macroscopic appearance similar to the corresponding CNF fiber (Figure 5a). Regarding the ability to bind IgG, a distinct green fluorescence signal from bound IgG can be seen from the CNF/Z-silk fiber (Figure 5b, middle panel) but not from the pure CNF or CNF/FN-silk fibers (Figure 5b, left and right panel, respectively). For the films, this indicates exposed and correctly folded Z domains in the composite CNF/Z-silk fibers.

Compared to the films, a slightly different behavior was observed when cells were cultured on the fibers. Before being

DOI: 10.1021/acsnano.7b02305
ACS Nano 2017, 11, 5148−5159

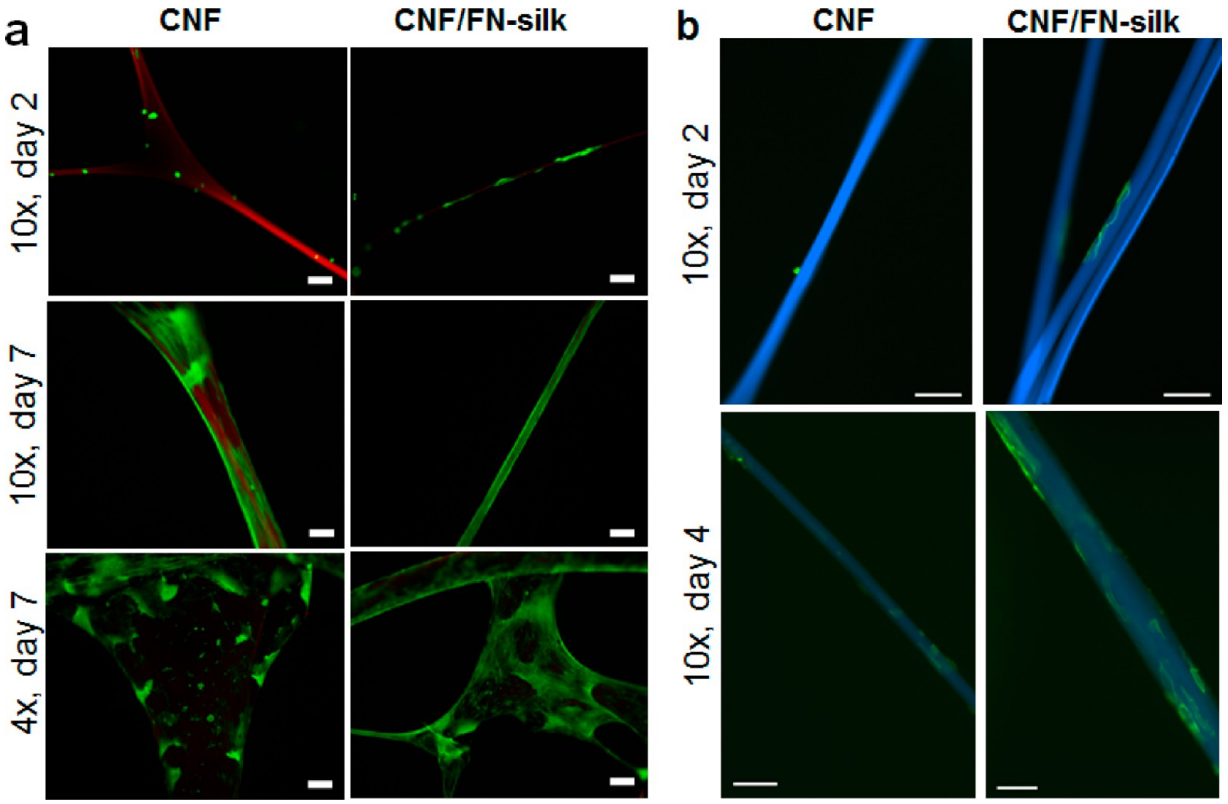

Figure 6. Cell adhesion to fibers. (a) Live/dead staining of human dermal fibroblasts growing on CNF (left panel) or CNF/FN-silk fibers (right panel) after 2 days (top panel) or 7 days culture (middle and bottom panels). Green, living cells; bright red, dead cells; dim red, autofluorescence from CNF. (b) F-actin staining (green) of endothelial cells after 2 days (top panel) and 4 days (bottom panel) of culture adhering to CNF (left panel) or CNF/FN-silk fibers (right panel). Dim blue: autofluorescence from CNF. Scale bars 250 μm for 4× and 100 μm for 10×.

seeded with cells, the fibers were mounted on sterile metal frames and placed in cell culture plates. Whereas cells were clearly not prone to adhere to the pure CNF films, fibers made of pure CNF supported some attachment and spreading, although to a lesser extent than the CNF/FN-silk fibers. Fibroblasts were found spreading along the CNF/FN-silk fiber, already after 2 days in culture, whereas on CNF fibers, a few viable but rounded cells with no signs of spreading were found at this early point (Figure 6a,b, top panels). However, after 7 days of culture, the fibroblasts were found spread out also along the pure CNF fibers, although still growing in clusters, indicating somewhat poor conditions for attachment (Figure 6a, middle and bottom panels).

The oriented pure CNF fibers thus seem to support attachment of fibroblasts better than the randomly oriented network of fibrils in the pure CNF film. This might partly be explained by differences in morphology; the film contains nanofibrils (diameter 3−10 nm) distributed with random orientations (Figure 1c), while the aligned CNF fibrils in the fibers give rise to both nano- and microstructures (0.2−0.3 μm) in the same direction (Figure 3a). Such structures might promote both adhesion of ECM proteins secreted to the culture media and subsequent adhesion of cells.[53] A high confluence and even distribution of fibroblasts were found on the CNF/FN-silk fibers, which *via* the silk module is decorated with ECM motifs already from the start.

Further, the fibers were seeded with endothelial cells, and the adhesion and spreading of these were analyzed by staining for F-actin. After 2 days of culture, only very few and rounded endothelial cells were found on fibers of pure CNF (Figure 6b), whereas the cells were found spread out along the fibers of CNF/FN-silk. After 4 days of culture, some endothelial cells were found spread out also on the pure CNF fibers, although less than on the CNF/FN-silk fibers. Thus, in both formats, the presence of the cell-binding motif FN linked to the silk dramatically adds a favorable cell adhesion property to the CNF materials. The high viability among all cells present on both fibers and films, with or without FN-silk, suggests that the CNF is indeed cytocompatible although not in itself promoting cell adherence.

CONCLUSIONS

Herein, we demonstrate a fairly simple, controllable, and industrially scalable manufacturing process for composites of CNF and RSP with elevated mechanical properties and biofunctionalities. Our results show significant progress in two complementary directions. First, in the field of biomaterials science, an attempt to interconnect the attractive properties of CNF and spider silk proteins resulted in high-performance structural and functional materials. Whereas inclusion of Z-silk proteins gives rise to significant improvement in tensile strength of CNF fibers, incorporation of both Z-silk and FN-silk proteins in CNF results in extraordinary bioactivity. Second, we established an engineering approach to nanostructuring, where the potentials of the nanoscale building blocks are utilized toward the synthesis of high-performance macroscopic materials. Moreover, a similar methodology can be adopted to create multifunctional materials from other polymer

DOI: 10.1021/acsnano.7b02305
ACS Nano 2017, 11, 5148−5159

building blocks. We believe that current results will lead to the development of lightweight composite materials from silk and cellulose, by breaking the limitations in terms of cost, mechanical properties (stiffness, strength and toughness), and biofunctionalities.

METHODS

Preparation of CNF. CNF dispersion was prepared by a protocol similar to that described by Håkansson *et al.*[41] Chemically bleached softwood fibers (a mixture of 60% Norwegian spruce and 40% Scots pine, Domsjo AB, Sweden) were used for liberating CNF. The content of carboxyl groups (COO^-) in the CNF dispersion is 0.6 mmol/g with an average length distribution of 400−600 nm and height of 2−3 nm (Figure S6).

Flow Setup. The flow setup consists of three syringe pumps (WPI, Al-4000), a double flow-focusing channel, and a bath, where the outlet is submerged. Syringe pumps were used to control the flow in the channels. The flow rates were 4.1 mL h^{-1} for the core flow (CNF or CNF/silk) and 4.7 and 24.9 mL h^{-1} for the first (H_2O) and second (pH-2 HCl) sheath flows, respectively. The flow channel was machined in a 1 mm thick stainless steel plate and sandwiched between two plexiglass plates. The plexiglass and channel plates were held together by two aluminum plates screwed together (Figure 3a). All the channels in the double flow-focusing geometry were 1 mm in width.

Preparation of Composite CNF/Silk Films and Fibers. CNF films were casted from a CNF dispersion (50 μL, 3.0 mg mL^{-1}) onto Teflon sheets and were allowed to air-dry at ambient temperature. Composite CNF/Z-silk and CNF/FN-silk films (50 μL, 2.7 mg mL^{-1} CNF, 0.3 mg mL^{-1} Z-silk or FN-silk) were prepared in the same way. Z-silk and FN-silk were produced in *Escherichia coli* and purified essentially as described elsewhere.[17,54,55] Fibers of CNF, CNF/Z-silk, and CNF/FN-silk (2.7 mg mL^{-1} CNF, 0.3 mg mL^{-1} Z-silk or FN-silk) were fabricated using double flow-focusing geometry. The fibers were collected in a water bath, winded up on a metal frame, and allowed to air-dry at ambient temperature. The macroscopic appearances of films and fibers were documented by optical microscopy.

Preparation of Composite CNF/Z Films and Coatings. Composite CNF/Z films (50 μL, 2.7 mg mL^{-1} CNF, 0.063 mg mL^{-1} Z) were casted onto Teflon sheets and air-dried at ambient temperature. Control CNF/Z-silk and CNF films were prepared as previously stated. The amount of Z molecules in the CNF/Z films was equimolar to the amount of Z-silk in the CNF/Z-silk films. For preparation of CNF/Z coatings, CNF films were first casted as previously described. After air-drying, the CNF films were immersed (dip-coated) in a Z protein solution (0.063 mg mL^{-1}) for 15 min at ambient temperature. Following removal of the unbound Z solution, films were incubated with 20 mM Tris (pH 8) buffer for 15 min at ambient temperature, followed by washing three times with Tris buffer and air-drying. Control CNF/Z-silk and CNF coatings were prepared in the same way by instead coating CNF films with Z-silk (0.3 mg mL^{-1}) and Tris buffer, respectively.

Binding of IgG to CNF/Z-silk. Air-dried CNF/Z-silk films and fibers were wetted in phosphate-buffered saline (PBS, pH 7.4), followed by incubation with rabbit anti-mouse IgG-Alexa Fluor 488 conjugate (0.05 mg mL^{-1}, Thermo Fisher Scientific) containing 0.5% (v/v) Tween 20 for 30 min at ambient temperature. Films and fibers were washed at least three times with PBS/0.5% Tween 20 buffer. Fluorescence microscopy was conducted for wet films and wet or dried fibers. Films and fibers of CNF and CNF/FN-silk were used as controls and treated in the same way.

Binding of IgG to CNF/Z. Binding of rabbit anti-mouse IgG-Alexa Fluor 488 conjugate to air-dried CNF/Z films and coatings was performed as previously described for CNF/Z-silk. As controls, films and coatings of CNF/Z-silk and CNF were used and treated in the same way.

Electron Microscopy Characterization and Tensile-Test Measurements. Transmission electron microscopy (TEM) imaging to study the CNF morphology was performed with a JEOL JEM-1400 TEM (Hitachi HT-7700, Japan) at 120 kV. Images were acquired with a Ruby camera following "systematic, uniform, random" rule to avoid bias for the size measurement. Prior to observation, the CNF dispersion (0.005% (w/v)) was deposited on a carbon-coated copper grid treated with glow discharge and stained with 2% uranyl acetate solution. Surface structure analysis of films and fibers was performed using SEM (Hitachi S-4800, Japan), and samples were prepared by sputtering the surface with a few nanometer-thin gold−palladium layers (Gressington Instruments Ltd., UK). The mechanical properties of the films were measured using an Instron 5944 instrument equipped with a 500 N load cell and for the fibers using an Instron E1000 instrument with a 5 N load cell. Samples were conditioned at 23 °C and 50% relative humidity (RH) for at least 24 h prior to testing. The dimensions of the samples were measured by an optical microscope. For a few fibers, cross sections were further cross-checked with SEM. The span length was 8−12 mm, and measurements were performed at a pulling rate of 2 mm min^{-1} for the films and 0.5 mm min^{-1} for the fibers. Tensile test results are averaged over at least 10 samples for each case.

Atomic Force Microscopy. Silicon wafers from Addison Engineering Inc. (San José, CA, USA) were oxidized at 1000 °C for 1 h to form a silica layer. The wafers were washed in Milli-Q, ethanol, and Milli-Q, dried, and treated in the plasma cleaner (PCD 002, Harrick Scientific Corp., Ossining, NY, USA) for 5 min to render the surface hydrophilic. Wafers with the size of 5 × 5 mm were covered with CNF and CNF/silk dispersions with the same concentration used for the fabrication of films and were left to dry in air at room temperature overnight. The prepared wafers were imaged using MultiMode 8 AFM (Bruker, Santa Barbara, CA, USA) using SCANASYST-AIR cantilevers. The roughness was measured for nonflattened images and is presented as the root mean square value. Height was 20 nm for CNF and CNF/Z-silk films and 32 nm for CNF/FN-silk films.

Fourier Transform Infrared Spectroscopy and Rheology. Attenuated total reflectance Fourier transform infrared (ATR-FTIR) spectroscopy was recorded in region of 3900 to 1000 cm^{-1} in absorbance mode using a platinum ATR unit from Bruker (Tensor 37) for both films and fibers.

Rheology measurements to investigate the viscoelastic properties of CNF and CNF/silk gels were carried out at room temperature using a DHR-2 rheometer (TA Instruments) with a 25 mm diameter parallel plate setup with a truncation gap of 300 μm. After placing 200 mL of dispersion between the plates, 1 mL of pH 2 HCl was added along the circumference to get gelation (Figure S7). Afterward, 0.25% strain was applied, and measurements of storage and loss modulus were carried out for a period of 45 min (until the time a constant measurement value was reached). After that, fractured stress was measured with increasing strain from 0.01 to 200% at a constant frequency of 1 Hz.

WAXS Measurement. The WAXS measurement was carried out at P03 beamline at Petra 3 at DESY, Hamburg.[56] Measurement for the quantification of the alignment of crystal planes into the fibers was performed at an X-ray wavelength of 0.95 Å. The sample-to-detector distance was set to 110 mm, and the beam size was 6 × 14 μm^2 (horizontal × vertical). A Pilatus 300-k detector (Dectris) with pixel size of 172 × 172 μm^2 was used.

Optical and Fluorescence Microscopy. Visual documentation of films and fibers was performed by optical microscopy using a stereomicroscope (Nikon) with a portable USB camera. Fluorescence microscopy of IgG-fluorophore binding and cellular stainings was conducted using an inverted Nikon Eclipse T*i* fluorescence microscope. IgG-Alexa Fluor 488 was excited at 455−490 nm and detected at 500−540 nm. Excitation at 488 nm and detection at 530−550 nm were used to monitor green fluorescence, whereas excitation at 543 nm and detection at 605−650 nm were used for red fluorescence. DAPI was detected by excitation at 405 nm and detection at 415−475 nm.

Culture of Fibroblasts and Endothelial Cells. Primary human dermal fibroblasts from juvenile foreskin (HDF) (ECACC) were cultured in DMEM F12 ham (Sigma) supplemented with 5% fetal bovine serum (Sigma) and 1% penicillin−streptomycin (VWR). Cells were expanded for 7 days after thawing, and cell viability was checked

DOI: 10.1021/acsnano.7b02305
ACS Nano 2017, 11, 5148−5159

with trypan blue prior to seeding at 20 000 viable cells/cm^2. All experiments were performed in passage 8−13.

For endothelial cell (EC) culture, the human dermal microvascular endothelial cells (HDMECs) isolated from dermis were used (PromoCell GmbH, Germany). First the EC were expanded and cultured on gelatin-coated flasks (0.1%, Sigma-Aldrich). Endothelial cell basal medium MV2 (PromoCell) with all supplements was used. The EC were seeded at passage 6−8 with a density of 25 000 cells/cm^2.

Live/Dead Staining. Live/dead viability assay (Molecular Probes Invitrogen, Carlsbad, CA, USA) was used to visualize living and dead cells on the matrices. This is a two-color fluorescence cell viability assay based on the simultaneous identification of living and dead cells with two probes (calcein acetoxymethyl ester (calcein-AM) and ethidium homodimer-1 (EthD-1)), reporting on intracellular esterase activity and plasma membrane integrity, respectively. The intracellular esterase activity in living cells is determined by the enzymatic conversion of the virtually nonfluorescent cell-permeable calcein-AM to the intensely green fluorescent calcein. EthD-1 enters cells with damaged membranes and undergoes a 40-fold enhancement of fluorescence upon binding to nucleic acids, producing a bright red fluorescence in the nuclei of dead cells. The matrices with cells were washed twice with prewarmed PBS before staining with calcein-AM and EthD-1 in complete medium for 30 min at room temperature.

Filamentous Actin Staining. The filamentous actin in the cells was visualized by staining with Phalloidin. Matrices with cells were washed twice in prewarmed PBS, fixed with 4% paraformaldehyde, and permeabilized with 0.1% Triton X-100 in PBS, before staining with Phalloidin conjugated with Alexa Fluor 488 (Invitrogen), diluted 1:40 in PBS. DAPI diluted 1:1000 was used for nuclear staining.

Enumeration of Cells Bound to Films. HDMECs (20 000/cm^2) were seeded onto CNF film with or without FN and fixed after 2, 4, or 6 days of culture with 4% PFA after gentle washing with prewarmed PBS. Nuclei and F-actin were stained with DAPI and Phalloidin−Alexa Fluor 488, and images were taken at 10× magnification after mounting under coverslips with fluorescence mounting medium (DAKO) using an inverted Nikon Eclipse T*i* fluorescence microscope. Number of DAPI-stained nuclei in each image was counted manually using the manual count tool in NIS elements Br and expressed as number of cells per area (A = 1 mm^2). Student's t-test was used for statistical evaluation.

ASSOCIATED CONTENT

Supporting Information

The Supporting Information is available free of charge on the ACS Publications website at DOI: 10.1021/acsnano.7b02305.

SEM images of the CNF/silk film surfaces (Figure S1); schematic illustration of the principle for IgG-fluorophore binding to Z-silk (Figure S2); free-standing CNF films with and without FN-silk after 7 days culture with HDMECs (Figure S3); rheology data for strain and angular frequency sweeps (Figure S4); SEM images of the CNF/silk fiber surfaces (Figure S5); length and height characterization of CNF fibrils (Figure S6); schematic of the gel formation procedure from the dispersions on a rheometer (Figure S7) (PDF)

AUTHOR INFORMATION

Corresponding Authors

*E-mail: myh@kth.se.

*E-mail: dansod@kth.se.

ORCID

Tobias Benselfelt: 0000-0003-4388-8970

My Hedhammar: 0000-0003-0140-419X

L. Daniel Söderberg: 0000-0003-3737-0091

Author Contributions

M.H., F.L., and L.D.S. conceived and directed the research. N.M., R.J., and M.W. fabricated the films and fibers with assistance from K.M.O.H. N.M. performed the mechanical testing and SEM characterization. N.M., F.L., and L.D.S. performed the WAXS measurement and analyzed the X-ray data. R.J. performed the experiments on the affinity properties. M.W. performed the cell adhesion experiments. M.H. supervised the research on bioactivity. N.M. performed the rheology measurements. T.B. and N.M. performed the AFM measurements. N.M. and R.J. performed the FTIR measurements. All authors contributed to interpreting the data and preparing the manuscript.

Notes

The authors declare no competing financial interest.

ACKNOWLEDGMENTS

This work is supported by FORMAS, The Swedish Research Council, Vinnova, Knut and Alice Wallenberg Foundation, and Wallenberg Wood Science Center at KTH. Farhan Ansari, Selina Parvin, Michaela Salajkova, Tahani Kaldeus, Andreas Barth, Irene Linares Arregui, and Tobias Ingverud are thanked for experimental assistance, and Pan Chen for VMD simulations. Spiber Technologies AB is acknowledged for providing soluble Z-silk and FN-silk proteins. Soluble Z protein was kindly provided by Sara Kanje. Stephan Roth and Peng Zhang from the P03 beamline at Petra 3, DESY, are acknowledged for assistance with the WAXS measurement.

REFERENCES

(1) Wegst, U. G. K.; Bai, H.; Saiz, E.; Tomsia, A. P.; Ritchie, R. O. Bioinspired Structural Materials. *Nat. Mater.* **2014**, *14*, 23−36.

(2) Keten, S.; Xu, Z.; Ihle, B.; Buehler, M. J. Nanoconfinement Controls Stiffness, Strength and Mechanical Toughness of [Beta]-Sheet Crystals in Silk. *Nat. Mater.* **2010**, *9*, 359−367.

(3) Wang, Y.; Kim, H. J.; Vunjak-Novakovic, G.; Kaplan, D. L. Stem Cell-based Tissue Engineering with Silk Biomaterials. *Biomaterials* **2006**, *27*, 6064−6082.

(4) Perrone, G. S.; Leisk, G. G.; Lo, T. J.; Moreau, J. E.; Haas, D. S.; Papenburg, B. J.; Golden, E. B.; Partlow, B. P.; Fox, S. E.; Ibrahim, A. M. S.; Lin, S. J.; Kaplan, D. L. The Use of Silk-Based Devices for Fracture Fixation. *Nat. Commun.* **2014**, *5*, 3385.

(5) Olsson, R. T.; Azizi Samir, M. A. S.; Salazar Alvarez, G.; Belova, L.; Ström, V.; Berglund, L. A.; Ikkala, O.; Nogues, J.; Gedde, U. W. Making Flexible Magnetic Aerogels and Stiff Magnetic Nanopaper Using Cellulose Nanofibrils as Templates. *Nat. Nanotechnol.* **2010**, *5*, 584−588.

(6) Morán, J. I.; Alvarez, V. A.; Cyras, V. P.; Vázquez, A. Extraction of Cellulose and Preparation of Nanocellulose from Sisal Fibers. *Cellulose* **2008**, *15*, 149−159.

(7) Xia, X. X.; Qian, Z. G.; Ki, C. S.; Park, Y. H.; Kaplan, D. L.; Lee, S. Y. Native-Sized Recombinant Spider Silk Protein Produced in Metabolically Engineered Escherichia Coli Results in a Strong Fiber. *Proc. Natl. Acad. Sci. U. S. A.* **2010**, *107*, 14059−14063.

(8) Lazaris, A.; Arcidiacono, S.; Huang, Y.; Zhou, J. F.; Duguay, F.; Chretien, N.; Welsh, E. A.; Soares, J. W.; Karatzas, C. N. Spider Silk Fibers Spun from Soluble Recombinant Silk Produced in Mammalian Cells. *Science* **2002**, *295*, 472−476.

(9) Spiess, K.; Lammel, A.; Scheibel, T. Recombinant Spider Silk Proteins for Applications in Biomaterials. *Macromol. Biosci.* **2010**, *10*, 998−1007.

(10) Huemmerich, D.; Slotta, U.; Scheibel, T. Processing and Modification of Films Made from Recombinant Spider Silk Proteins. *Appl. Phys. A: Mater. Sci. Process.* **2006**, *82*, 219−222.

(11) Fredriksson, C.; Hedhammar, M.; Feinstein, R.; Nordling, K.; Kratz, G.; Johansson, J.; Huss, F.; Rising, A. Tissue Response to

DOI: 10.1021/acsnano.7b02305
ACS Nano 2017, 11, 5148−5159

Subcutaneously Implanted Recombinant Spider Silk: An *In Vivo* Study. *Materials* **2009**, *2*, 1908.
(12) Widhe, M.; Johansson, J.; Hedhammar, M.; Rising, A. Current Progress and Limitations of Spider Silk for Biomedical Applications. *Biopolymers* **2012**, *97*, 468−478.
(13) Omenetto, F. G.; Kaplan, D. L. New Opportunities for an Ancient Material. *Science* **2010**, *329*, 528−531.
(14) Vendrely, C.; Scheibel, T. Biotechnological Production of Spider-Silk Proteins Enables New Applications. *Macromol. Biosci.* **2007**, *7*, 401−409.
(15) Schacht, K.; Scheibel, T. Processing of Recombinant Spider Silk Proteins into Tailor-Made Materials for Biomaterials Applications. *Curr. Opin. Biotechnol.* **2014**, *29*, 62−69.
(16) Widhe, M.; Johansson, U.; Hillerdahl, C. O.; Hedhammar, M. Recombinant Spider Silk with Cell Binding Motifs for Specific Adherence of Cells. *Biomaterials* **2013**, *34*, 8223−8234.
(17) Jansson, R.; Thatikonda, N.; Lindberg, D.; Rising, A.; Johansson, J.; Nygren, P. Å.; Hedhammar, M. Recombinant Spider Silk Genetically Functionalized with Affinity Domains. *Biomacromolecules* **2014**, *15*, 1696−1706.
(18) Jansson, R.; Courtin, C. M.; Sandgren, M.; Hedhammar, M. Rational Design of Spider Silk Materials Genetically Fused with an Enzyme. *Adv. Funct. Mater.* **2015**, *25*, 5343−5352.
(19) Gomes, S.; Leonor, I. B.; Mano, J. F.; Reis, R. L.; Kaplan, D. L. Spider Silk-Bone Sialoprotein Fusion Proteins for Bone Tissue Engineering. *Soft Matter* **2011**, *7*, 4964−4973.
(20) Wong, C.; Kaplan, D. L. Genetic Engineering of Fibrous Proteins: Spider Dragline Silk and Collagen. *Adv. Drug Delivery Rev.* **2002**, *54*, 1131−1143.
(21) Wohlrab, S.; Müller, S.; Schmidt, A.; Neubauer, S.; Kessler, H.; Leal-Egaña, A.; Scheibel, T. Cell Adhesion and Proliferation on RGD-Modified Recombinant Spider Silk Proteins. *Biomaterials* **2012**, *33*, 6650−6659.
(22) Klemm, D.; Kramer, F.; Moritz, S.; Lindström, T.; Ankerfors, M.; Gray, D.; Dorris, A. Nanocelluloses: A New Family of Nature-Based Materials. *Angew. Chem., Int. Ed.* **2011**, *50*, 5438−5466.
(23) Berglund, L. A.; Peijs, T. Cellulose Biocomposites—From Bulk Moldings to Nanostructured Systems. *MRS Bull.* **2010**, *35*, 201−207.
(24) McKee, J. R.; Huokuna, J.; Martikainen, L.; Karesoja, M.; Nykänen, A.; Kontturi, E.; Tenhu, H.; Ruokolainen, J.; Ikkala, O. Molecular Engineering of Fracture Energy Dissipating Sacrificial Bonds Into Cellulose Nanocrystal Nanocomposites. *Angew. Chem., Int. Ed.* **2014**, *53*, 5049−5053.
(25) Abdul Khalil, H. P. S.; Bhat, A. H.; Ireana Yusra, A. F. Green Composites from Sustainable Cellulose Nanofibrils: A Review. *Carbohydr. Polym.* **2012**, *87*, 963−979.
(26) Malho, J. M.; Arola, S.; Laaksonen, P.; Szilvay, G. R.; Ikkala, O.; Linder, M. B. Modular Architecture of Protein Binding Units for Designing Properties of Cellulose Nanomaterials. *Angew. Chem., Int. Ed.* **2015**, *54*, 12025−12028.
(27) Lin, N.; Dufresne, A. Nanocellulose in Biomedicine: Current Status and Future Prospect. *Eur. Polym. J.* **2014**, *59*, 302−325.
(28) Walther, A.; Bjurhager, I.; Malho, J. M.; Pere, J.; Ruokolainen, J.; Berglund, L. A.; Ikkala, O. Large-Area, Lightweight and Thick Biomimetic Composites with Superior Material Properties *via* Fast, Economic, and Green Pathways. *Nano Lett.* **2010**, *10*, 2742−2748.
(29) Nilsson, B.; Moks, T.; Jansson, B.; Abrahmsén, L.; Elmblad, A.; Holmgren, E.; Henrichson, C.; Jones, T. A.; Uhlén, M. A Synthetic IgG-binding Domain Based on Staphylococcal Protein A. *Protein Eng., Des. Sel.* **1987**, *1*, 107−113.
(30) Widhe, M.; Shalaly, N. D.; Hedhammar, M. A Fibronectin Mimetic Motif Improves Integrin Mediated Cell Biding to Recombinant Spider Silk Matrices. *Biomaterials* **2016**, *74*, 256−266.
(31) Shahzadi, K.; Mohsin, I.; Wu, L.; Ge, X.; Jiang, Y.; Li, H.; Mu, X. Bio-Based Artificial Nacre with Excellent Mechanical and Barrier Properties Realized by a Facile *In Situ* Reduction and Cross-Linking Reaction. *ACS Nano* **2017**, *11*, 325−334.
(32) Aulin, C.; Salazar-Alvarez, G.; Lindstrom, T. High Strength, Flexible and Transparent Nanofibrillated Cellulose-Nanoclay Biohybrid Films with Tunable Oxygen and Water Vapor Permeability. *Nanoscale* **2012**, *4*, 6622−6628.
(33) Henriksson, M.; Berglund, L. A.; Isaksson, P.; Lindström, T.; Nishino, T. Cellulose Nanopaper Structures of High Toughness. *Biomacromolecules* **2008**, *9*, 1579−1585.
(34) Nishiyama, Y.; Langan, P.; Chanzy, H. Crystal Structure and Hydrogen-Bonding System in Cellulose Iβ from Synchrotron X-ray and Neutron Fiber Diffraction. *J. Am. Chem. Soc.* **2002**, *124*, 9074−9082.
(35) Tashiro, M.; Tejero, R.; Zimmerman, D. E.; Celda, B.; Nilsson, B.; Montelione, G. T. High-Resolution Solution NMR Structure of the Z Domain of Staphylococcal Protein A1. *J. Mol. Biol.* **1997**, *272*, 573−590.
(36) Zhang, Y.; Carbonell, R. G.; Rojas, O. J. Bioactive Cellulose Nanofibrils for Specific Human IgG Binding. *Biomacromolecules* **2013**, *14*, 4161−4168.
(37) Torres-Rendon, J. G.; Köpf, M.; Gehlen, D.; Blaeser, A.; Fischer, H.; Laporte, L. D.; Walther, A. Cellulose Nanofibril Hydrogel Tubes as Sacrificial Templates for Freestanding Tubular Cell Constructs. *Biomacromolecules* **2016**, *17*, 905−913.
(38) Lou, Y. R.; Kanninen, L.; Kuisma, T.; Niklander, J.; Noon, L. A.; Burks, D.; Urtti, A.; Yliperttula, M. The Use of Nanofibrillar Cellulose Hydrogel As a Flexible Three-Dimensional Model to Culture Human Pluripotent Stem Cells. *Stem Cells Dev.* **2014**, *23*, 380−392.
(39) Bhattacharya, M.; Malinen, M. M.; Lauren, P.; Lou, Y. R.; Kuisma, S. W.; Kanninen, L.; Lille, M.; Corlu, A.; GuGuen-Guillouzo, C.; Ikkala, O.; Laukkanen, A.; Urtti, A.; Yliperttula, M. Nanofibrillar Cellulose Hydrogel Promotes Three-Dimensional Liver Cell Culture. *J. Controlled Release* **2012**, *164*, 291−298.
(40) Mertaniemi, H.; Escobedo-Lucea, C.; Sanz-Garcia, A.; Gandía, C.; Mäkitie, A.; Partanen, J.; Ikkala, O.; Yliperttula, M. Human Stem Cell Decorated Nanocellulose Threads for Biomedical Applications. *Biomaterials* **2016**, *82*, 208−220.
(41) Håkansson, K. M. O.; Fall, A. B.; Lundell, F.; Yu, S.; Krywka, C.; Roth, S. V.; Santoro, G.; Kvick, M.; Prahl Wittberg, L.; Wågberg, L.; Söderberg, L. D. Hydrodynamic Alignment and Assembly of Nanofibrils Resulting in Strong Cellulose Filaments. *Nat. Commun.* **2014**, *5*, 4018.
(42) Barth, A. Infrared Spectroscopy of Proteins. *Biochim. Biophys. Acta, Bioenerg.* **2007**, *1767*, 1073−1101.
(43) Schacht, K.; Scheibel, T. Controlled Hydrogel Formation of a Recombinant Spider Silk Protein. *Biomacromolecules* **2011**, *12*, 2488−2495.
(44) Torres-Rendon, J. G.; Schacher, F. H.; Ifuku, S.; Walther, A. Mechanical Performance of Macrofibers of Cellulose and Chitin Nanofibrils Aligned by Wet-Stretching: A Critical Comparison. *Biomacromolecules* **2014**, *15*, 2709−2717.
(45) Lundahl, M. J.; Cunha, A. G.; Rojo, E.; Papageorgiou, A. C.; Rautkari, L.; Arboleda, J. C.; Rojas, O. J. Strength and Water Interactions of Cellulose I Filaments Wet-Spun from Cellulose Nanofibril Hydrogels. *Sci. Rep.* **2016**, *6*, 30695.
(46) Iwamoto, S.; Isogai, A.; Iwata, T. Structure and Mechanical Properties of Wet-Spun Fibers Made from Natural Cellulose Nanofibers. *Biomacromolecules* **2011**, *12*, 831−836.
(47) Walther, A.; Timonen, J. V. I; Díez, I.; Laukkanen, A.; Ikkala, O. Multifunctional High-Performance Biofibers Based on Wet-Extrusion of Renewable Native Cellulose Nanofibrils. *Adv. Mater.* **2011**, *23*, 2924−2928.
(48) Tang, H.; Butchosa, N.; Zhou, Q. A Transparent, Hazy, and Strong Macroscopic Ribbon of Oriented Cellulose Nanofibrils Bearing Poly(ethylene glycol). *Adv. Mater.* **2015**, *27*, 2070−2076.
(49) Zhu, H.; Zhu, S.; Jia, Z.; Parvinian, S.; Li, Y.; Vaaland, O.; Hu, L.; Li, T. Anomalous Scaling Law of Strength and Toughness of Cellulose Nanopaper. *Proc. Natl. Acad. Sci. U. S. A.* **2015**, *112*, 8971−8976.
(50) Foo, C. W. P.; Bini, E.; Hensman, J.; Knight, D. P.; Lewis, R. V.; Kaplan, D. L. Role of pH and Charge on Silk Protein Assembly in Insects and Spiders. *Appl. Phys. A: Mater. Sci. Process.* **2006**, *82*, 223−233.

DOI: 10.1021/acsnano.7b02305
ACS Nano 2017, 11, 5148−5159

(51) Rammensee, S.; Slotta, U.; Scheibel, T.; Bausch, A. R. Assembly Mechanism of Recombinant Spider Silk Proteins. *Proc. Natl. Acad. Sci. U. S. A.* **2008**, *105*, 6590−6595.
(52) Hajian, A.; Lindström, S. B.; Pettersson, T.; Hamedi, M. M.; Wågberg, L. Understanding the Dispersive Action of Nanocellulose for Carbon Nanomaterials. *Nano Lett.* **2017**, *17*, 1439−1447.
(53) Bettinger, C. J.; Langer, R.; Borenstein, J. T. Engineering Substrate Topography at the Micro- and Nanoscale to Control Cell Function. *Angew. Chem., Int. Ed.* **2009**, *48*, 5406−5415.
(54) Hedhammar, M.; Rising, A.; Grip, S.; Martinez, A. S.; Nordling, K.; Casals, C.; Stark, M.; Johansson, J. Structural Properties of Recombinant Nonrepetitive and Repetitive Parts of Major Ampullate Spidroin 1 from Euprosthenops Australis: Implications for Fiber Formation. *Biochemistry* **2008**, *47*, 3407−3417.
(55) Hedhammar, M.; Bramfeldt, H.; Baris, T.; Widhe, M.; Askarieh, G.; Nordling, K.; Aulock, S. v.; Johansson, J. Sterilized Recombinant Spider Silk Fibers of Low Pyrogenicity. *Biomacromolecules* **2010**, *11*, 953−959.
(56) Buffet, A.; Rothkirch, A.; Döhrmann, R.; Körstgens, V.; Abul Kashem, M. M.; Perlich, J.; Herzog, G.; Schwartzkopf, M.; Gehrke, R.; Müller-Buschbaum, P.; Roth, S. V. P03, The Microfocus and Nanofocus X-ray Scattering (MiNaXS) Beamline of the PETRA III Storage Ring: The Microfocus Endstation. *J. Synchrotron Radiat.* **2012**, *19*, 647−653.

DOI: 10.1021/acsnano.7b02305
ACS Nano 2017, 11, 5148−5159